Structures of Ceftazidime and Its Transition-State Analogue in Complex with AmpC β-Lactamase: Implications for Resistance Mutations and Inhibitor Design[†,‡]

Rachel A. Powers,[§] Emilia Caselli,[||] Pamela J. Focia,[§] Fabio Prati,[||] and Brian K. Shoichet*[,§]

Department of Molecular Pharmacology and Biological Chemistry, Northwestern University, 303 East Chicago Avenue, Chicago, Illinois 60611, and Dipartimento di Chimica, Università degli Studi di Modena, Via Campi 183, Modena, Italy

Received May 8, 2001; Revised Manuscript Received June 7, 2001

ABSTRACT: Third-generation cephalosporins are widely used β-lactam antibiotics that resist hydrolysis by β-lactamases. Recently, mutant β-lactamases that rapidly inactivate these drugs have emerged. To investigate why third-generation cephalosporins are relatively stable to wild-type class C β-lactamases and how mutant enzymes might overcome this, the structures of the class C β-lactamase AmpC in complex with the third-generation cephalosporin ceftazidime and with a transition-state analogue of ceftazidime were determined by X-ray crystallography to 2.0 and 2.3 Å resolution, respectively. Comparison of the acyl-enzyme structures of ceftazidime and loracarbef, a β-lactam substrate, reveals that the conformation of ceftazidime in the active site differs from that of substrates. Comparison of the structures of the acyl-enzyme intermediate and the transition-state analogue suggests that ceftazidime blocks formation of the tetrahedral transition state, explaining why it is an inhibitor of AmpC. Ceftazidime cannot adopt a conformation competent for catalysis due to steric clashes that would occur with conserved residues Val211 and Tyr221. The X-ray crystal structure of the mutant β-lactamase GC1, which has improved activity against third-generation cephalosporins, suggests that a tandem tripeptide insertion in the Ω loop, which contains Val211, has caused a shift of this residue and also of Tyr221 that would allow ceftazidime and other third-generation cephalosporins to adopt a more catalytically competent conformation. These structural differences may explain the extended spectrum activity of GC1 against this class of cephalosporins. In addition, the complexed structure of the transition-state analogue inhibitor (K_i 20 nM) with AmpC reveals potential opportunities for further inhibitor design.

Third-generation cephalosporins, such as ceftazidime, are widely used as antibiotics, especially against nosocomial bacterial infections. The popularity of these β-lactams is partly explained by their stability to β-lactamase enzymes, which are the most widespread resistance mechanism against the β-lactam family of antibiotics. Unfortunately, mutant β-lactamases have arisen that can rapidly hydrolyze these drugs, threatening their utility. The bases of the stability of these drugs to most wild-type serine β-lactamases, and how mutant enzymes overcome this stability, have been intensely studied (*1*−*9*).

Knox and colleagues have recently determined the X-ray crystal structures of one of these clinically isolated mutant enzymes, a class C β-lactamase GC1 from *Enterobacter cloacae*, both in the apo form (*6*) and in complex with a novel mechanism-based inhibitor (*9*). GC1 β-lactamase contains a tandem tripeptide insertion in the Ω loop region that confers extended substrate activity against most third-generation cephalosporins, which have traditionally been resistant to hydrolysis by β-lactamases (*2*). The apo structure shows that this insertion increases the flexibility of the Ω loop and widens the binding site by as much as 1.4 Å (*6*). In the structure of the GC1/inhibitor complex, an active site tyrosine, corresponding to residue 221, is displaced by 6 Å, opening the active site even further (*9*). It was proposed that these changes might allow the entry of larger substituents into the active site, enable the acyl-enzyme intermediate to be better positioned for attack by the deacylating water molecule, or allow for easier departure of the hydrolyzed product (*6*). However, it was not clear from the crystal structures how these changes actually increase hydrolysis of third-generation cephalosporins, since a structure of GC1, or indeed any β-lactamase, in complex with one of these compounds has not been determined.

In an effort to correlate these structural changes with enzyme activity against third-generation cephalosporins, we determined the structures of ceftazidime (Figure 1A) and a boronic acid transition-state analogue inhibitor with the R1 side chain of ceftazidime (compound **1**; Figure 1B) bound to the wild-type class C β-lactamase AmpC from *Escherichia coli*. We reasoned that comparing these structures with the GC1 structures would help to explain the higher activity of the mutant GC1 enzyme. Furthermore, we have previously

[†] Supported by Grant GM63815 from the NIH (to B.K.S.). We thank the American Chemical Society Division of Medicinal Chemistry and Bristol-Myers Squibb for a predoctoral fellowship (to R.A.P.). This work was partly conducted at the Stanford Synchrotron Radiation Laboratory (SSRL), which is funded by the Department of Energy (BES, BER) and the National Institutes of Health (NCRR, NIGMS).

[‡] The coordinates and structure factors for the AmpC/ceftazidime and AmpC/**1** complexes have been deposited in the Protein Data Bank with the accession codes 1IEL and 1IEM, respectively.

* To whom correspondence should be addressed. Phone: 312-503-0081. Fax: 312-503-5349. E-mail: b-shoichet@northwestern.edu.

[§] Northwestern University.

[||] Università degli Studi di Modena.

10.1021/bi0109358 CCC: $20.00
Published on Web 07/10/2001

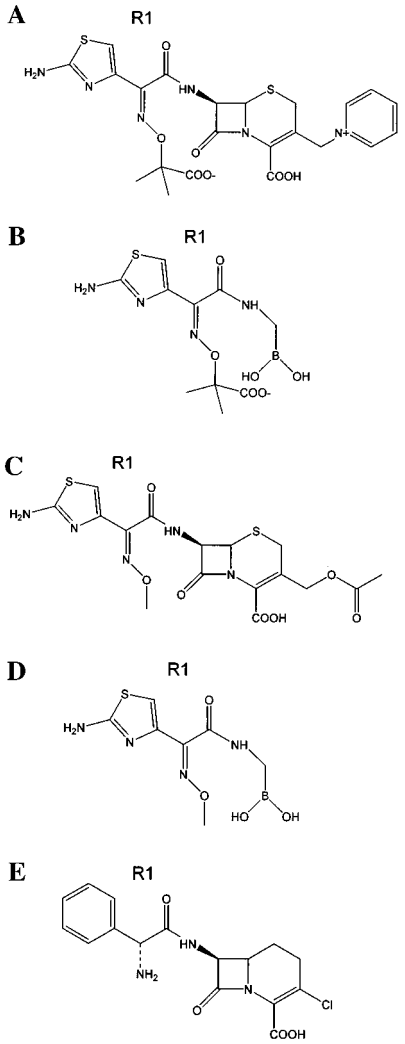

FIGURE 1: Chemical structures of β-lactamase ligands: (A) ceftazidime, a third-generation cephalosporin; (B) compound **1**, a boronic acid inhibitor bearing the R1 side chain from ceftazidime (*10*); (C) cefotaxime, a third-generation cephalosporin; (D) compound **2**, a boronic acid inhibitor bearing the R1 side chain from cefotaxime; (E) loracarbef, a β-lactam substrate.

found that compound **1** is a potent inhibitor of AmpC (K_i 20 nM) that reverses resistance in cell culture (*10*), making the structure of the AmpC/**1** complex also interesting from an inhibitor design perspective.

Here we report the X-ray crystal structures of ceftazidime and **1**, each in complex with AmpC (Figure 2). AmpC is 70% identical and 82% homologous with GC1, and the structures of the two enzymes closely resemble each other (RMSD[1] of 0.81 Å for all common Cα atoms). These structures help to explain why ceftazidime resists hydrolysis by wild-type class C β-lactamases and how GC1 overcomes this resistance, leading to its extended spectrum activity. The structure of the boronic acid analogue also suggested a further direction for inhibitor design, which we investigated through synthesis and kinetic characterization of a new analogue.

MATERIALS AND METHODS

Synthesis. Compound **1** was synthesized as described previously (*10*). Pinacol [[2-amino-α-methoxyimino-4-thiazolylacetyl]amino]methane boronate (compound **2**; Figure 1D) was synthesized as follows. Isobutyl chloroformate (233 μL, 1.8 mmol) was added to a solution of (*Z*)-2-amino-α-methoxyimino-4-thiazoleacetic acid (366 mg, 1.8 mmol) in anhydrous dimethylformamide (2 mL) at −10 °C and allowed to react under inert atmosphere; after 10 min, anhydrous triethylamine (250 μL, 1.8 mmol) was added and allowed to react for 2 h. Thereafter, a solution of pinacol bis(trimethylsilyl)aminomethane boronate (602 mg, 2 mmol) in anhydrous tetrahydrofuran (2 mL), previously treated with anhydrous methanol (2 mmol), was added at the same temperature. After 20 min, the temperature was raised to room temperature, and the mixture was allowed to react for 16 h. The white precipitate (ammonium chloride) was centrifuged, and the solvent was evaporated under reduced pressure. The residue was crystallized from $CHCl_3$/*n*-hexane to give the desired product as a white crystalline solid (32%, mp 107−110 °C dec). ^{1}H NMR ($CDCl_3$): δ 1.32 (12H, s, CH_3), 1.72 (2H, br, NH_2), 3.01 (2H, d, J = 4.6 Hz, CH_2-NH), 4.06 (3H, s, OCH_3), 6.22 (1H, br, N*H*), 7.06 (1H, s, ar). ^{13}C NMR ($CDCl_3$): δ 25.2, 63.5, 84.7, 113.0, 143.9, 149.8, 163.4, 168.2. MS: *m*/*z* 340 (M^+), 325, 309, 282, 251, 209, 208, 183, 166, 141, 126 (base peak), 125, 98, 83, 59, 55.

Crystal Growth and Structure Determination. AmpC from *E. coli* was expressed, purified to homogeneity, and crystallized in 1.7 M potassium phosphate (pH 8.7), as described (*11*). Native AmpC crystals were harvested using nylon loops, placed in a 6 μL drop of 50 mM ceftazidime and 1.7 M potassium phosphate (pH 8.7) solution, and soaked for 30 min to obtain the acyl-enzyme complex of ceftazidime with AmpC. Ceftazidime was a gift from Jesús Blázquez.

Cocrystals of AmpC/**1** were grown by vapor diffusion in hanging drops equilibrated over 1.7 M potassium phosphate buffer (pH 8.7) using microseeding techniques. The initial concentration of protein in the drop was 95 μM, and the concentration of the inhibitor was 586 μM. The inhibitor was added to the crystallization drop in a 2% dimethyl sulfoxide (DMSO) and 1.7 M potassium phosphate buffer (pH 8.7) solution. Crystals appeared within 3−5 days after equilibration at 23 °C.

Data were measured on beam line 7-1 at the Stanford Synchrotron Radiation Laboratory at 100 K using a Mar345 image plate detector. Prior to data collection, cocrystals of AmpC/**1** were immersed in a cryoprotectant solution of 20% sucrose and 1.7 M potassium phosphate, pH 8.7, for about 20 s and then flash cooled in liquid nitrogen. AmpC crystals soaked with ceftazidime were immersed in a cryoprotectant solution of 20% sucrose, 50 mM ceftazidime, and 1.7 M potassium phosphate, pH 8.7, for about 20 s and then flash cooled in liquid nitrogen. Each data set was measured from a single crystal.

Reflections were indexed, integrated, and scaled using the HKL package (*12*) (Table 1). The space group was *C*2, with two AmpC molecules in the asymmetric unit. In the structure of AmpC/**1**, each AmpC molecule contained 358 residues. In the structure of AmpC/ceftazidime, molecule 2 of the asymmetric unit contained 358 residues, and molecule 1 contained 355 residues; residues 284, 285, and 290 were excluded from the final model due to poor electron density in this region. The structures were determined by molecular replacement using an AmpC/boronic acid complexed struc-

[1] Abbreviations: RMSD, root mean square deviation; DMSO, dimethyl sulfoxide; PBP, penicillin-binding protein.

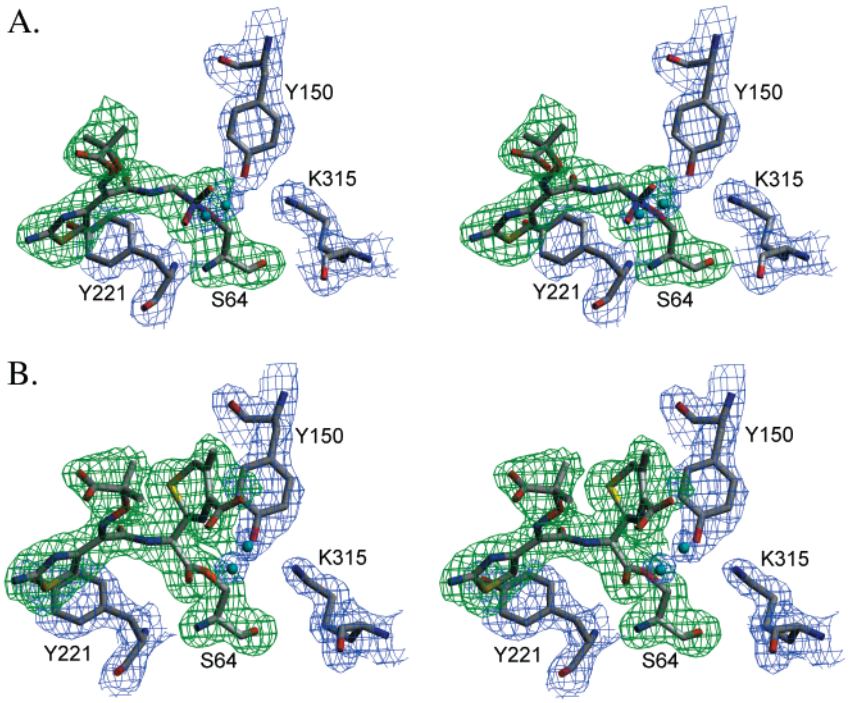

FIGURE 2: Stereoview of the refined models of AmpC in complex with (A) compound **1** and (B) ceftazidime. $2F_o - F_c$ electron density maps are shown in blue, contoured at 1.0σ. A simulated-annealing omit map of each ligand is shown in green, contoured at 3.2σ for **1** and 3.0σ for ceftazidime. Carbon atoms are colored gray, nitrogen atoms blue, oxygen atoms red, sulfur atoms yellow, and boron atoms purple. Water molecules are represented as cyan spheres. This figure was generated using SETOR (*29*).

Table 1: Data Collection and Refinement Statistics

	AmpC/**1**	AmpC/ceftazidime
cell constants (Å; deg)	a =118.56, b = 78.06, c = 97.24; β = 115.44	a = 118.49, b = 77.04, c = 98.07; β = 115.76
resolution (Å)	2.30 (2.38−2.30)[a]	2.00 (2.07−2.00)[a]
unique reflections	35024	46338
total observations	137203	152381
R_{merge} (%)	7.5 (35.9)[a]	5.8 (23.8)[a]
completeness (%)[b]	98.8 (99.9)[a]	86.5 (99.9)[a]
$\langle I\rangle/\langle\sigma_I\rangle$	11.2 (4.0)[a]	14.8 (6.4)[a]
resolution range for refinement (Å)	20−2.3	20−2.0
no. of protein residues	716	713
no. of water molecules	209	277
RMSD bond lengths (Å)	0.009	0.011
RMSD bond angles (deg)	1.5	1.6
R-factor (%)	18.2	18.2
R_{free} (%)	22.8[c]	22.6[d]
av *B*-factor		
protein atoms (Å^2)	32.4[e]	27.5[e]
protein atoms (Å^2, monomer 1 only)	31.0	28.6
protein atoms (Å^2, monomer 2 only)	34.1	28.2
inhibitor atoms (Å^2)	44.5[e]	42.5[e]
inhibitor atoms (Å^2, monomer 1 only)	40.2	40.9
inhibitor atoms (Å^2, monomer 2 only)	48.8	44.2

[a] Values in parentheses are for the highest resolution shell. [b] Fraction of theoretically possible reflections observed. (Interference from ice rings resulted in resolution bins that were less complete.) [c] R_{free} was calculated with 6% of reflections set aside randomly. [d] R_{free} was calculated with 5% of reflections set aside randomly. [e] Values cited were calculated for both molecules in the asymmetric unit.

ture (PDB entry 1FSY) (*10*), with inhibitor and water molecules removed, as the initial phasing model. Both structures were refined using the maximum likelihood target in CNS and included simulated annealing, positional, and individual temperature factor refinement with a bulk solvent correction (*13*). Sigma A-weighted electron density maps were calculated with CNS and used in steps of manual rebuilding using the program O (*14*). For each model, the inhibitors were built into the initial observed difference density in each active site of the asymmetric unit, and the structures of the complexes were further refined using CNS (Table 1).

Enzyme Inhibition Assays. Stock solutions of the inhibitor were made up in DMSO at 10 mM, and subsequent 10-fold or 100-fold stock dilutions were made as necessary. Enzyme inhibition assays were performed using cephalothin as a substrate and were monitored at 265 nm as described previously (*15*). All reactions were initiated by enzyme in an HP8453 UV/visible spectrophotometer with multicell transport running HP ChemStation software (version 2.5). IC_{50} values were determined at 100 μM substrate concentration. The K_i value for compound **2** was obtained by comparison of progress curves in the presence and absence of inhibitor (*16*).

RESULTS

The X-ray crystal structures of both the β-lactam ceftazidime and the boronic acid inhibitor bearing the R1 side chain from ceftazidime, compound **1**, were determined in complex with the class C β-lactamase AmpC to 2.0 and 2.3 Å resolution, respectively (Table 1, Figure 2). Unambiguous electron density in the initial $F_o - F_c$ maps (contoured at 3σ) revealed the location and conformation of each inhibitor in the active sites. Simulated-annealing omit maps of the refined models confirmed the placement of each inhibitor in the active sites.

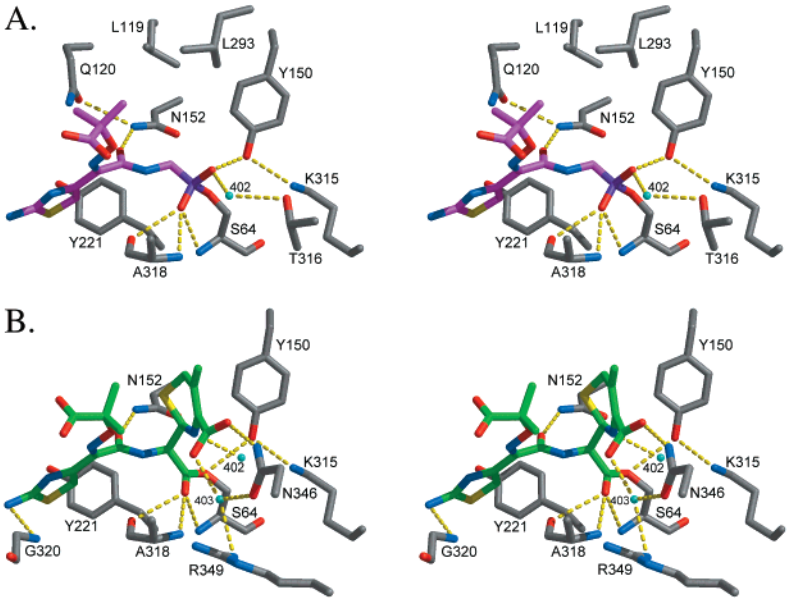

FIGURE 3: Interactions observed between AmpC and bound ligands: (A) compound **1**; (B) ceftazidime. Dashed yellow lines indicate distances between 2.5 and 3.2 Å. Atoms are colored as in Figure 2, except carbon atoms of **1** are in magenta and carbon atoms of ceftazidime are in green. This figure and Figures 4−6 were generated with MidasPlus (*30*).

The quality of each of the models was analyzed with the program Procheck (*17*). For the AmpC/**1** complex, 90.0% of the non-proline, non-glycine residues were in the most favored region of the Ramachandran plot (10.0% in the additionally allowed region); for the AmpC/ceftazidime complex, 91.4% of the non-proline, non-glycine residues were in the most favored region (8.6% in the additionally allowed region).

In the complex of AmpC with **1**, electron density is observed connecting Oγ of the catalytic Ser64 with the boron atom of the inhibitor (Figure 2A). The geometry around the boron atom is tetrahedral, as expected, since the inhibitor is a deacylation transition-state analogue (*18*). Several interactions are observed in this complex that are conserved in other complexes between AmpC and boronic acid derivatives. Three hydrogen bonds are made with the O1 hydroxyl of **1** (Figure 3A; see Table 2 for atom numbering), which corresponds to the oxygen of the deacylation transition state bound in the "electrophilic" (*11*) or "oxyanion" (*19*) hole. Two of these hydrogen bonds are with the main chain nitrogen atoms of Ser64 and Ala318 (3.0 and 2.9 Å, respectively), and the third is with the main chain oxygen of Ala318 (3.0 Å). The O2 hydroxyl of **1**, which is thought to correspond to the deacylating water in the deacylation high-energy intermediate, hydrogen bonds with the hydroxyl of Tyr150 (2.5 Å) and a well-ordered water molecule (Wat402, 2.5 Å). A hydrogen bond is observed between Wat402, which is thought to represent the deacylating water prior to nucleophilic attack, and Wat403 (2.6 Å), another well-ordered water molecule. In addition, Wat402 interacts with Oγ1 of Thr316 (2.9 Å). Consistent with earlier structures (*10*), the carbonyl oxygen of the amide group (O12) forms a hydrogen bond with Nδ2 of Asn152 (2.6 Å; Figure 3A). Both Asn152 on the enzyme and this amide group on the R1 side chains of β-lactams are highly conserved.

Unexpectedly, the unique portion of the R1 side chain makes relatively few direct interactions with the protein. The thiazole ring of **1** makes van der Waals or quadrupole−quadrupole interactions with Tyr221; C15 of the inhibitor is 3.8 Å from the center of the tyrosine ring. The methyl group C20 interacts with the hydrophobic patch formed by Leu119

Table 2: Interactions in Complexed and Native AmpC β-Lactamase

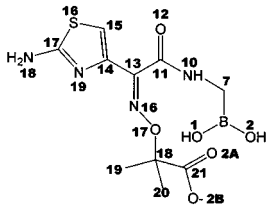

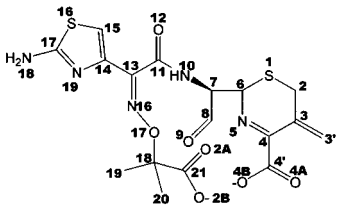

	distance (Å)		
interaction	AmpC/**1**[a]	AmpC/ceftazidime[a]	native AmpC[b]
S64N−O1/O9	3.0	2.8	NP[c]
A318N−O1/O9	2.9	2.7	NP
A318O−O1/O9	3.0	3.1	NP
Y150OH−O2	2.5	NP	NP
Wat402−O2	2.5	NP	NP
Wat402−N5	NP	2.6	NP
Y150OH−K315Nζ	2.9	2.8	2.5
Y150OH−S64Oγ	2.8	3.0	3.2
Y150OH−K67Nζ	3.3	2.6	3.1
K67Nζ−A220O	2.8	3.4	3.5
K67Nζ−S64Oγ	2.6	3.0	3.5
Wat402−T316Oγ1	2.9	3.4	3.8[d]
Wat402−Wat403	2.6	4.2	NP
Wat403−N346Oδ1	2.7	2.8	NP
Wat403−R349Nη1	3.2	3.0	NP
Wat403−O4A	NP	2.6	NP
N346Nδ2−O4B	NP	2.8	NP
A318O−N10	3.6	3.4	NP
N152Nδ2−O12	2.6	2.8	NP
Q120Nϵ2−O12	3.6	6.7	NP
N152Oδ1−K67Nζ	2.6	2.6	2.7
N152Nδ2−Q120Oϵ1	3.2	6.9	3.0
Q120Oϵ1−Wat440	2.6	NP	NP
N18−G320N	3.3	3.2	NP
N289Cβ−C3′	NP	3.8	NP

[a] Distances are for monomer 1 of the asymmetric unit. [b] Distances are for monomer 2 of the asymmetric unit. [c] Not present. [d] In the native structure, Wat402 is called Wat387.

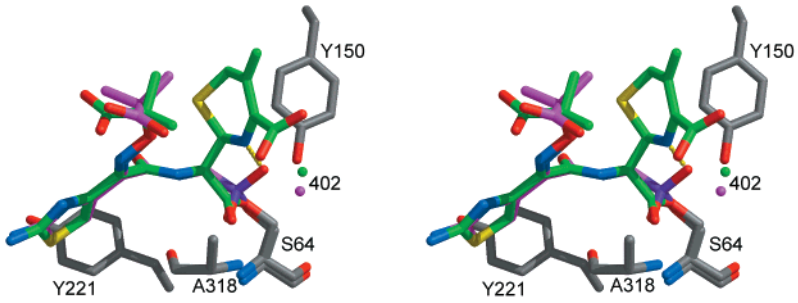

FIGURE 4: Stereoview of an overlay of **1** with ceftazidime. Atoms are colored as in Figure 3. The distance between the O2 hydroxyl of **1** and N5 of ceftazidime is 1.8 Å (dashed yellow line). Spheres representing Wat402 from each structure are colored magenta from the AmpC/**1** structure and green from the AmpC/ceftazidime structure.

and Leu293 (4.2 Å to Cδ2 of Leu119 and 4.1 Å to Cδ1 of Leu293). The C21 carboxylate group of the R1 side chain points toward bulk solvent. This dimethyl/carboxylate moiety may be somewhat flexible in the site, as indicated by its higher *B*-factors and poor electron density as compared with the rest of the inhibitor. Nearby residues that might provide interactions with this carboxylate are Asn343 (3.4 Å from Nδ2 to O2B) and Asn289 (4.5 Å from Nδ2 to O2B). The amino group (N18) of the thiazole ring of **1** forms a long hydrogen bond with the main chain nitrogen of Gly320 (3.3 Å).

In the AmpC/ceftazidime complex, continuous electron density connects Oγ of Ser64 and C7 of ceftazidime (Figure 2B). The geometry around this carbon atom is planar, as expected for an acyl-enzyme complex. The carbonyl oxygen O9 of the opened lactam ring is pointing into the electrophilic (*11*) or oxyanion (*19*) hole and hydrogen bonds with the main chain nitrogen atoms of Ser64 and Ala318 (2.8 and 2.7 Å, respectively; Figure 3B). As observed in other β-lactamase/β-lactam complexes (*9*, *20*−*23*), a presumably unfavorable interaction is observed between O9 and the main chain oxygen of Ala318 (3.1 Å). In the acyl-enzyme complex, ceftazidime folds back on itself, such that C19 of the R1 side chain is within van der Waals contact of C2 and C3 of the cephalosporin ring; these distances are in the range of 3.9−4.1 Å (Figure 3B). These internal interactions reduce the exposure of the hydrophobic portions of the molecule to solvent.

The interactions made by the R1 side chain of ceftazidime resemble those made by its analogous R1 side chain in **1**. The carbonyl oxygen of the R1 amide group (O12) hydrogen bonds with Asn152 (2.8 Å; Figure 3B). Also observed are the quadrupole−quadrupole interactions made between the thiazole ring and Tyr221 (4.0 Å from C15 to the center of Tyr221). The methyl group C19 points into the hydrophobic patch formed by Leu119 and Leu293, but it is slightly farther away from these residues than in the complex with **1** (4.8 Å from C19 to Leu119Cδ2). The carboxylate group of the R1 side chain points toward bulk solvent. As in the AmpC/**1** complex, this portion of the compound seems to be flexible; the electron density is diminished, and the *B*-factors are higher than those observed for the rest of the molecule. As with **1**, multiple conformations could be assumed by this flexible portion of ceftazidime. Residues that are near this carboxylate group are Asn343 (4.3 Å from Nδ2 to O2B), Arg204 (5.6 Å from Nη2 to O2B), and Gln120 (5.4 Å from Nϵ2 to O2A). As with **1**, the amino group (N18) of the thiazole ring of ceftazidime hydrogen bonds with the main chain nitrogen of Gly320 (3.2 Å).

On the other side of the ligand, the dihydrothiazine ring of ceftazidime makes several specific interactions with the enzyme (Figure 3B). The C4′ carboxylate hydrogen bonds with Nδ2 of Asn346 (2.8 Å to O4B) and with Nη1 of Arg349 via a water molecule (Wat403; O4A−Wat403 is 2.6 Å, and Wat403−Arg349Nη1 is 3.0 Å). Wat403 also hydrogen bonds with Oδ1 of Asn346 (2.8 Å). The nitrogen of the opened lactam ring (N5) hydrogen bonds with Wat402 (2.6 Å); this water is thought to represent the deacylating water molecule. The exocyclic carbon C3′ packs near the Cβ atom of Asn289 (3.8 Å).

We compared the structure of the acyl-enzyme complex (AmpC/ceftazidime) with its transition-state analogue complex (AmpC/**1**) (Figure 4). When the two complexes are superimposed using their Cα atoms, the shared R1 side chain of the two compounds differs by 1.2 Å RMSD for all 19 atoms of the side chain starting with atom C7. The major deviation arises from the different placement of atoms C19, C20, C21, O2A, and O2B, which also have the highest *B*-factors in both molecules. When these five atoms are left out, the RMSD becomes 0.5 Å. By comparison, for all atoms of active site residues Lys67, Tyr150, Asn152, Lys315, and Ala318, the RMSD distance is 0.4 Å between the two structures.

Compound **1** is a 20 nM inhibitor of AmpC, but the carboxylate-containing moiety of the R1 side chains of ceftazidime and **1** made few direct interactions with the enzyme. To investigate the role of this group, we synthesized a boronic acid analogue that lacked it, replacing it with the R1 side chain from cefotaxime (Figure 1C), another third-generation cephalosporin, giving compound **2** (Figure 1D). To our surprise, this inhibitor was found to have a K_i of 310 nM for AmpC, 15-fold worse than **1**. As has been shown in earlier studies with boronic acid inhibitors of serine β-lactamases (*10*, *15*, *16*), both **1** and **2** are reversible inhibitors of AmpC that show no time dependence to their inhibition. Unlike inhibition values for β-lactam inhibitors, the values for these transition-state analogues represent true K_i values.

DISCUSSION

Ceftazidime and related third-generation cephalosporins are widely used clinically because of their broad-spectrum antibiotic activity and their relative stability to many β-lactamases. By determining the crystal structures of AmpC in complex with ceftazidime and with a transition-state analogue of ceftazidime, we investigated the following questions: why are these compounds relatively resistant to hydrolysis by class C β-lactamases, how does the insertion mutant GC1 over-

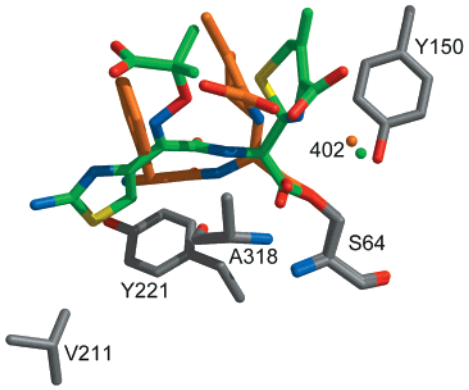

FIGURE 5: Overlay of ceftazidime with loracarbef, a β-lactam substrate. Atoms are colored as in Figure 3, except carbon atoms of loracarbef are in orange. Spheres representing Wat402 are colored green in the wild-type AmpC/ceftazidime structure and orange in the Q120L/Y150E AmpC/loracarbef structure.

come this, and why is the transition-state analogue (compound **1**) so potent an inhibitor of the wild-type enzyme?

Three models for β-lactam inhibition of serine β-lactamases have been proposed. One model suggests that β-lactam inhibitors displace the hydrolytic water molecule, preventing deacylation (*4*, *9*, *24*). In class C β-lactamases, the structure of the inhibitor cloxacillin with a mutant AmpC fits this model in that the C3′ carboxylate of the inhibitor is observed to displace the deacylating water (*22*). This is also true of the complex between the monobactam aztreonam and the class C β-lactamase from *Citrobacter freundii* (*25*)—an overlay of this structure with that of a substrate complex suggests that the putative catalytic water would be displaced by the sulfonate of aztreonam. A second model suggests that β-lactam inhibitors destabilize the formation of the deacylation high-energy intermediate by physically occluding the space where the transition state would develop (*9*, *22*). In this model, portions of the β-lactam—typically the lactam nitrogen itself—are forced into a position where they would sterically block the formation of the tetrahedral deacylation high-energy intermediate. In this model, the deacylating water may still be present, as long as the substrate is in a conformation where the tetrahedral transition state cannot form. The AmpC/cloxacillin structure and the aztreonam complex are also consistent with this model. Moreover, the structure of the inhibitor moxalactam with wild-type AmpC is consistent only with this model—the deacylating water remains present in the acyl adduct, but formation of the transition state appears blocked (*22*). The structure of GC1 in complex with a novel sulfone inhibitor also supports this model; the sulfinate group of the inhibitor appears to destabilize formation of the tetrahedral transition state (*9*). Finally, a third model suggests that an electronic rearrangement, which occurs within the acyl-adduct after lactam ring opening, makes third-generation cephalosporins relatively inert to water attack (*26*). Of these three models, only the first two are addressed by the present study.

A comparison of the AmpC complexes with ceftazidime and with the β-lactam substrate loracarbef (*22*) (Figure 1E) shows that the bound conformation of ceftazidime differs from that of the substrate (Figure 5). In apparent conflict with the first model, this orientation does not exclude the deacylating water molecule Wat402. Wat402 is observed in the active site of AmpC/ceftazidime, interacting with N5 of the opened lactam ring, although it is displaced by 1.2 Å relative to its position in the loracarbef structure. Conversely, a comparison of the structures of the acyl-enzyme intermediate and the deacylation transition-state analogue suggests that formation of the transition state is blocked in the ceftazidime complex (Figure 4). The O2 hydroxyl of **1** is thought to represent the position of the deacylating water, and the distance between O2 and N5 of the opened lactam ring of ceftazidime is 1.8 Å, too close for formation of the tetrahedral transition state represented in the structure of AmpC/**1**. It appears that ceftazidime is a poor substrate of AmpC because it destabilizes the high-energy tetrahedral intermediate, preventing rapid deacylation (*22*). Although *some* β-lactams are inhibitors because they displace the deacylating water (model 1 above), the structures of *all* of the β-lactamase/β-lactam inhibitor complexes determined so far [the class C enzyme from *C. freundii* with aztreonam (*25*), AmpC/moxalactam (*22*), AmpC/cloxacillin (*22*), GC1/sulfone (*9*), and AmpC/ceftazidime] are consistent with the second model. They all appear to destabilize formation of the tetrahedral transition state.

Why then does ceftazidime adopt a conformation that is incompetent for catalysis? When ceftazidime is modeled in a conformation similar to the catalytically competent conformation adopted by loracarbef, it collides with invariant residues Val211 and Tyr221 (Figure 6). The unfavorable interactions in this modeled conformation are between ceftazidime N18 and V211Cγ2 (2.3 Å), ceftazidime S16 and Y221Cδ1 (2.4 Å), and ceftazidime C15 and Y221Cδ1 (2.5 Å). These collisions appear to force ceftazidime away from the catalytically competent conformation, such that its dihydrothiazine ring is placed to block the formation of the high-energy tetrahedral intermediate. We note that, in the structure of the complex between the class C β-lactamase from *C. freundii* and the monobactam aztreonam (*25*), the R1 side chain is in a similar position to that adopted in the ceftazidime complex, and the same interactions are made between the aminothiazole rings, Tyr221, and Val211. Although the lactam cores between aztreonam and ceftazidime are quite different, their R1 side chains are identical. The R1 side chain may play an important role in placing the acyl-enzyme adduct in a position that is either competent or incompetent (inhibitory) for hydrolytic attack.

The activity of the mutant β-lactamase GC1 is consistent with this model. An overlay of the GC1 structure with the AmpC/ceftazidime complex suggests that in GC1 ceftazidime would be better able to adopt the conformation of a substrate (i.e., loracarbef) because the binding site has widened (Figure 6). Val211 in AmpC has in essence been replaced by Ala211 (the first residue of the tripeptide insertion) in GC1. Ala211 has shifted away from the binding site by approximately 1.5 Å (as measured by the Cα positions of residues Val211 and Ala211) (Figure 6). The insertion in the Ω loop also causes Tyr221 to shift by approximately 0.3 Å and rotate approximately 20° around the Cβ−Cγ bond. This change is even more apparent in the GC1/sulfone complex where the Ω loop has adopted a completely different conformation, displacing Tyr221 6 Å away from the active site. These changes result in an active site that can better accommodate the bulky R1 side chains of ceftazidime and other third-generation cephalosporins and indeed other β-lactams, such as aztreonam, that share the same R1 side chain. In turn,

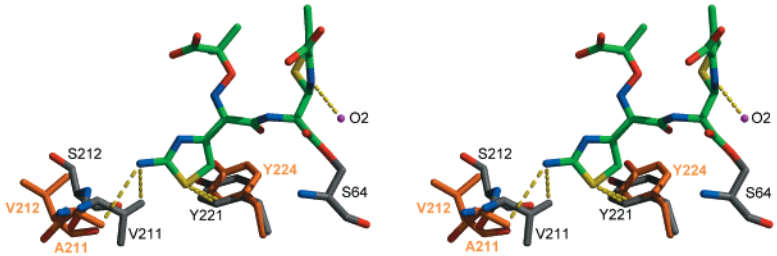

FIGURE 6: Stereoview of an overlay of AmpC/ceftazidime with unliganded GC1. Ceftazidime has been modeled into a catalytically competent conformation, similar to the conformation adopted by the substrate loracarbef (see Figure 5). The magenta sphere labeled O2 marks the location of the O2 hydroxyl atom from the AmpC/**1** structure and represents the putative location of the deacylating water in the high-energy intermediate. Atoms are colored as in Figure 3, except carbon atoms of GC1 are in orange. Residues Ala211 and Val212 of the tripeptide insertion in the ω loop of GC1 are shown; the third residue of the insertion Arg213 as well as residues Val214 and Ser215 is missing from the final model of GC1 due to poor density (*6*). Distances indicated by dashed yellow lines are as follows: N5−O2 = 2.5 Å; N18−V211Cγ2 (AmpC) = 2.3 Å; N18−A211Cβ (GC1) = 3.8 Å; S16−Y221Cδ1 (AmpC) = 2.4 Å; S16−Y224Cδ1 (GC1) = 2.7 Å.

this would allow the acyl-enzyme intermediate to relax into a conformation that would not destabilize the tetrahedral transition state during deacylation. Indeed, the distance between the O2 hydroxyl in the transition-state analogue complex and N5 of the opened lactam ring in the acyl-enzyme complex would be 2.5 Å in this modeled orientation, suggesting that the β-lactam itself might stabilize its own transition state, as has been previously suggested (*27*) and as is seen in the loracarbef complex (*22*).

One question not answered in a simple way by these complexes is why **1** is a 20 nM inhibitor of AmpC. This is 1000-fold more potent than a glycyl boronic acid that lacks the aminothiazole/oxime functionality characteristic of third-generation cephalosporins, and one naturally would expect to see key specificity interactions with this portion of the inhibitor. However, this side chain makes relatively few specific interactions in the crystal structure. The aminothiazole ring, which is characteristic of most third-generation cephalosporins, interacts in an edge-to-face manner with Tyr221, typical of quadrupole−quadrupole interactions. The dimethyl group off the oxime (C19 and C20; Table 2) makes nonpolar, hydrophobic contacts with Leu119 and Leu293. The carboxylate group of the side chain points into the bulk solvent.

To investigate what, if anything, the dimethyl/carboxylate moiety of the R1 side chain contributes to binding, we synthesized a boronic acid transition-state analogue that replaces this group with a methoxyimine (compound **2**; Figure 1D), which is the R1 side chain of cefotaxime. Both of these compounds inhibit reversibly, so that a comparison of K_i values reflects true energetic differences. The approximately 15-fold worse K_i value of **2** compared to **1** suggests that the dimethyl/carboxylate group does indeed contribute to the energy of binding. The hydrophobic interactions between the methyl groups and leucines 119 and 293 may account for most of this differential affinity. Also, based on the flexibility of this part of the molecule, the carboxylate group may interact favorably with polar residues in the site. Surprisingly, the aminothiazole ring, which is contained in almost all third-generation cephalosporins, contributes relatively little to binding compared to simpler side chains (e.g., that of cephalothin, compound **11** from ref *10*). We note that this aminothiazole group adopts a different conformation in the binding site of the R61 DD-peptidase, a small penicillin-binding protein (PBP), in its complex with cefotaxime (*28*). This owes to the intervention of a tryptophan (Trp233) in the DD-peptidase that is absent in AmpC. However much the aminothiazole group contributes to improved recognition of third-generation cephalosporins by PBPs, it seems that different β-lactam-recognizing enzymes can bind this characteristic group in substantially different ways.

Third-generation cephalosporins, like ceftazidime, are widely used clinically due to their relative inertness to β-lactamases. The crystal structures of ceftazidime and its transition-state analogue in complexes with AmpC suggest that these antibiotics are stable to the actions of class C β-lactamases because their bulky R1 side chain makes unfavorable interactions with the enzyme, specifically with residues Val211 and Tyr221. To relieve these interactions, these β-lactams rotate into a conformation that blocks formation of the deacylation high-energy intermediate; this conformation is incompetent for catalysis. The mutant class C β-lactamase GC1 appears to achieve its activity against third-generation cephalosporins by increasing the size of the active site, especially in the region of Val211 and Tyr221, relieving the high-energy interactions and allowing β-lactams such as ceftazidime to relax into a catalytically competent conformation. The X-ray crystal structure of AmpC in complex with **1**, a 20 nM inhibitor, may be a template for further inhibitor discovery against serine β-lactamases and their broad spectrum mutants.

ACKNOWLEDGMENT

We thank B. Beadle, X. Wang, S. McGovern, and I. Trehan for reading the manuscript.

REFERENCES

1. Raquet, X., Lamotte-Brasseur, J., Fonze, E., Goussard, S., Courvalin, P., and Frere, J. M. (1994) *J. Mol. Biol. 244*, 625−639.
2. Nukaga, M., Haruta, S., Tanimoto, K., Kogure, K., Taniguchi, K., Tamaki, M., and Sawai, T. (1995) *J. Biol. Chem. 270*, 5729−5735.
3. Maveyraud, L., Saves, I., Burlet-Schiltz, O., Swaren, P., Masson, J. M., Delaire, M., Mourey, L., Prome, J. C., and Samama, J. P. (1996) *J. Biol. Chem. 271*, 10482−10489.
4. Taibi-Tronche, P., Massova, I., Vakulenko, S. B., Lerner, S. A., and Mobashery, S. (1996) *J. Am. Chem. Soc. 118*, 7441−7448.
5. Banerjee, S., Pieper, U., Kapadia, G., Pannell, L. K., and Herzberg, O. (1998) *Biochemistry 37*, 3286−3296.
6. Crichlow, G. V., Kuzin, A. P., Nukaga, M., Mayama, K., Sawai, T., and Knox, J. R. (1999) *Biochemistry 38*, 10256−10261.

7. Vakulenko, S. B., Taibi-Tronche, P., Toth, M., Massova, I., Lerner, S. A., and Mobashery, S. (1999) *J. Biol. Chem. 274*, 23052−23060.
8. Tranier, S., Bouthors, A. T., Maveyraud, L., Guillet, V., Sougakoff, W., and Samama, J. P. (2000) *J. Biol. Chem. 275*, 28075−28082.
9. Crichlow, G. V., Nukaga, M., Doppalapudi, V. R., Buynak, J. D., and Knox, J. R. (2001) *Biochemistry 40*, 6233−6239.
10. Caselli, E., Powers, R. A., Blasczcak, L. C., Wu, C. Y., Prati, F., and Shoichet, B. K. (2001) *Chem. Biol. 8*, 17−31.
11. Usher, K. C., Blaszczak, L. C., Weston, G. S., Shoichet, B. K., and Remington, S. J. (1998) *Biochemistry 37*, 16082−16092.
12. Otwinowski, Z., and Minor, W. (1997) *Methods Enzymol. 276*, 307−326.
13. Brunger, A. T., Adams, P. D., Clore, G. M., DeLano, W. L., Gros, P., Grosse-Kunstleve, R. W., Jiang, J. S., Kuszewski, J., Nilges, M., Pannu, N. S., Read, R. J., Rice, L. M., Simonson, T., and Warren, G. L. (1998) *Acta Crystallogr. D 54*, 905−921.
14. Jones, T. A., Zou, J. Y., Cowan, S. W., and Kjeldgaard, M. (1991) *Acta Crystallogr. A 47*, 110−119.
15. Weston, G. S., Blazquez, J., Baquero, F., and Shoichet, B. K. (1998) *J. Med. Chem. 41*, 4577−4586.
16. Waley, S. G. (1982) *Biochem. J. 205*, 631−633.
17. Laskowski, R. A., MacArthur, M. W., Moss, D. S., and Thornton, J. M. (1993) *J. Appl. Crystallogr. 26*, 283−291.
18. Lobkovsky, E., Billings, E. M., Moews, P. C., Rahil, J., Pratt, R. F., and Knox, J. R. (1994) *Biochemistry 33*, 6762−6772.
19. Murphy, B. P., and Pratt, R. F. (1988) *Biochem. J. 256*, 669−672.
20. Strynadka, N. C., Adachi, H., Jensen, S. E., Johns, K., Sielecki, A., Betzel, C., Sutoh, K., and James, M. N. (1992) *Nature 359*, 700−705.
21. Maveyraud, L., Massova, I., Birck, C., Miyashita, K., Samama, J. P., and Mobashery, S. (1996) *J. Am. Chem. Soc. 118*, 7435−7440.
22. Patera, A., Blaszczak, L. C., and Shoichet, B. K. (2000) *J. Am. Chem. Soc. 122*, 10504−10512.
23. Kuzin, A. P., Nukaga, M., Nukaga, Y., Hujer, A., Bonomo, R. A., and Knox, J. R. (2001) *Biochemistry 40*, 1861−1866.
24. Matagne, A., Lamotte-Brasseur, J., Dive, G., Knox, J. R., and Frere, J. M. (1993) *Biochem. J. 293*, 607−611.
25. Oefner, C., D'Arcy, A., Daly, J. J., Gubernator, K., Charnas, R. L., Heinze, I., Hubschwerlen, C., and Winkler, F. K. (1990) *Nature 343*, 284−288.
26. Mazzella, L. J., and Pratt, R. F. (1989) *Biochem. J. 259*, 255−260.
27. Bulychev, A., Massova, I., Miyashita, K., and Mobashery, S. (1997) *J. Am. Chem. Soc. 119*, 7619−7625.
28. Kuzin, A. P., Liu, H., Kelly, J. A., and Knox, J. R. (1995) *Biochemistry 34*, 9532−9540.
29. Evans, S. V. (1993) *J. Mol. Graphics 11*, 134−138.
30. Ferrin, T. E., Huang, C. C., Jarvis, L. E., and Langridge, R. (1988) *J. Mol. Graphics 6*, 13−27.

BI0109358